Available online at www.sciencedirect.com
SCIENCE DIRECT®
International Journal of Heat and Mass Transfer 48 (2005) 4073–4089
International Journal of HEAT and MASS TRANSFER
www.elsevier.com/locate/ijhmt

Measurement and modeling of single-phase and flow-boiling heat transfer in microtubes

S. Grohmann *

CERN, CH-1211 Geneva 23, Switzerland

Received 25 October 2004; received in revised form 9 March 2005

Abstract

This paper presents an experimental technique and experimental results of heat transfer measurements in microtubes of 250 and 500 μm diameter. The data obtained with single-phase argon show no physical difference of heat transfer mechanisms between micro- and macrotubes. The enhancement of heat transfer compared to conventional correlations is explained with the increased influence of roughness, and modeled with a new relative roughness parameter. In two-phase flow, nucleate boiling heat transfer coefficients are lower than in macrotubes. An extension of the diameter dependence in the *VDI Wärmeatlas* correlation is proposed, and the conditions for stable flow-boiling are discussed.

Keywords: Boiling; Forced convection; Measurement techniques; Microscale; Modeling; Roughness

1. Introduction

Conventional correlations for modeling heat transfer in single- and two-phase flow are usually valid for tube diameters down to about 3–5 mm. Following a general trend for a more compact heat exchanger design and especially motivated by the requirements in electronics cooling, microchannel heat exchangers with hydraulic diameters of less than 1 mm have become a subject of intensive studies. So far, however, there is no generally accepted heat transfer model for this range, and recent publications are partially contradictory.

For example, both Qu et al. [1] and Rahman [2] investigated heat transfer during single-phase laminar flow in silicon microchannels. While Rahman measured higher Nusselt numbers than conventional correlations predict, Qu and his colleagues found generally lower Nusselt numbers. Both authors, however, conclude that the surface roughness was responsible for the deviations from conventional models, which are made for hydraulically smooth tubes.

In the case of single-phase turbulent flow, various authors reported that the heat transfer in microtubes is superior to the predictions made with conventional correlations. Adams et al. [3,4] compared their experimental data with results from Yu et al. [5]. They correlated increasing deviations towards smaller tube diameters and proposed an enhancement factor for the Gnielinski equation [6]. The effect of roughness, however, was not studied in detail.

In two-phase flow, a comprehensive review of recent literature on flow-boiling in small channels is given by Kandlikar [7–9]. He concludes that, as a first order

* Present address: Forschungszentrum Karlsruhe, Institute for Technical Physics, P.O. Box 3640, D-76021 Karlsruhe, Germany. Tel.: +49 7247 82 35 20; fax: +49 7247 82 28 49.
E-mail address: steffen.grohmann@itp.fzk.de

0017-9310/$ - see front matter © 2005 Elsevier Ltd. All rights reserved.
doi:10.1016/j.ijheatmasstransfer.2005.04.008

Nomenclature

A	surface area
d	diameter
g	acceleration due to gravity
k	overall heat transfer coefficient
L	length
$\mathscr{L}$	Laplace constant
$\dot{m}$	mass flow
$\dot{M}$	mass flux
Nu	Nusselt number
p	pressure
P	perimeter
Pr	Prandtl number
$\dot{q}$	heat flux
$\dot{Q}$	heat flow
r_d	relative roughness parameter
R	thermal resistance
R_a	arithmetic mean roughness
Re	Reynolds number
T	temperature
x	fluid quality

Greek symbols

α	heat transfer coefficient
ϵ	relative roughness
η	dynamic viscosity
λ	thermal conductivity
ρ	density
σ	surface tension

Subscripts

0	reference value
∞	far-field value
c	at the critical point, cross-sectional, convection
crit	critical value
eff	effective
fl	fluid
in	inlet
l	liquid phase
lam	at laminar flow
m	mean value
nb	nucleate boiling
onb	onset of nucleate boiling
s	saturation
out	outlet
turb	at turbulent flow
v	vapor phase
w	at the wetted surface

estimate, microchannel heat transfer may be predicted with flow-boiling correlations developed for large diameter tubes. Petterson [10] came to the same conclusion after broad studies on flow-boiling of CO_2 in parallel microchannel tubes of 0.8 mm inner diameter. He used several heat transfer models to fit his experimental data, and found the best agreement with the pool boiling correlation of the *VDI Wärmeatlas* edited by Gorenflo [11].

Peng et al. [12], on the other hand, claimed that flow-boiling in microchannels can be quite different from heat transfer in macrotubes. They indicated that regular nucleate boiling does not exist, and introduced new concepts of "fictitious boiling", "critical bubble size" and "evaporating space". These hypotheses, however, were disproved by various experimental results, such as the data published by Zhang [13]. Other authors, for example Zhao [14], concluded that the two-phase heat transfer coefficient in microtubes is substantially higher than in macrotubes. Large flow instabilities in parallel microchannels were observed by a number of authors. Peles et al. [15] even stated that two-phase flow in microchannels is inherently instable.

Most published studies on two-phase cooling in microtubes were conducted on application-oriented samples with parallel flow channels of various shapes (see [15–18]), or on single enhanced-surface channels documented by Zhang et al. [13]. However, there are few quantitative data that allow the modeling of two-phase heat transfer in tubes or channels below 500 μm diameter, which is the interesting size for package-integrated electronics cooling.

The experiments presented in this paper were therefore carried out with circular microtubes of 250 and 500 μm diameter, and with a single flow path to avoid negative impacts due to flow instabilities and maldistribution. The heat transfer studies were part of a Ph.D. project [19] on cooling of low-temperature tracking detectors, carried out within the RD39 Collaboration at CERN [20–22].

Fig. 1 shows a prototype silicon detector module developed by RD39, which has a 5×6 cm microstrip sensor that is operated at around 130 K. The 1.8 W heat load dissipated by 6 APV25[1] readout ASICs[2] is absorbed in a 500 μm microtube heat exchanger, using two-phase flow of argon. The integration of the heat exchanger close to the heat sources minimizes the amount of conductive material needed for heat spreading, and the overall impact ("visibility") of the cooling system in the module.

[1] 128-channel CMOS chip for the CMS experiment.
[2] Application-specific integrated circuit.

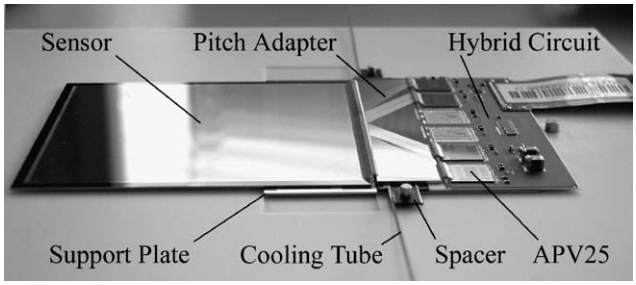

Fig. 1. Prototype of a cryogenic silicon detector module [25].

2. Experimental set-up and method

2.1. Experimental set-up

The experimental set-up used for heat transfer measurements in microtubes at cryogenic temperatures is shown schematically in Fig. 2. The working fluid was circulated in a closed circuit, which consisted of a warm and a cold part. The warm part comprised a compressor unit, a filtering system, a flowmeter, and some gas handling components. The cold part of the circuit was installed in a vacuum chamber operated under 10^{-6} mbar insulating vacuum. It was connected to the warm part through an internal heat exchanger, and consisted of a thermal interface, an electrical pre-heater, and a test section. The thermal interface was attached to the cold finger of a cryocooler, which was the heat sink that provided the cooling power. All cold circuit components were surrounded by a thermal radiation shield that was heat sinked to the cryocooler.

The thermal interface consisted of a condenser and a reservoir in the upper volume, and a sub-cooler heat exchanger in the lower volume. The reservoir was operated under saturation (liquid/vapor phase equilibrium). The

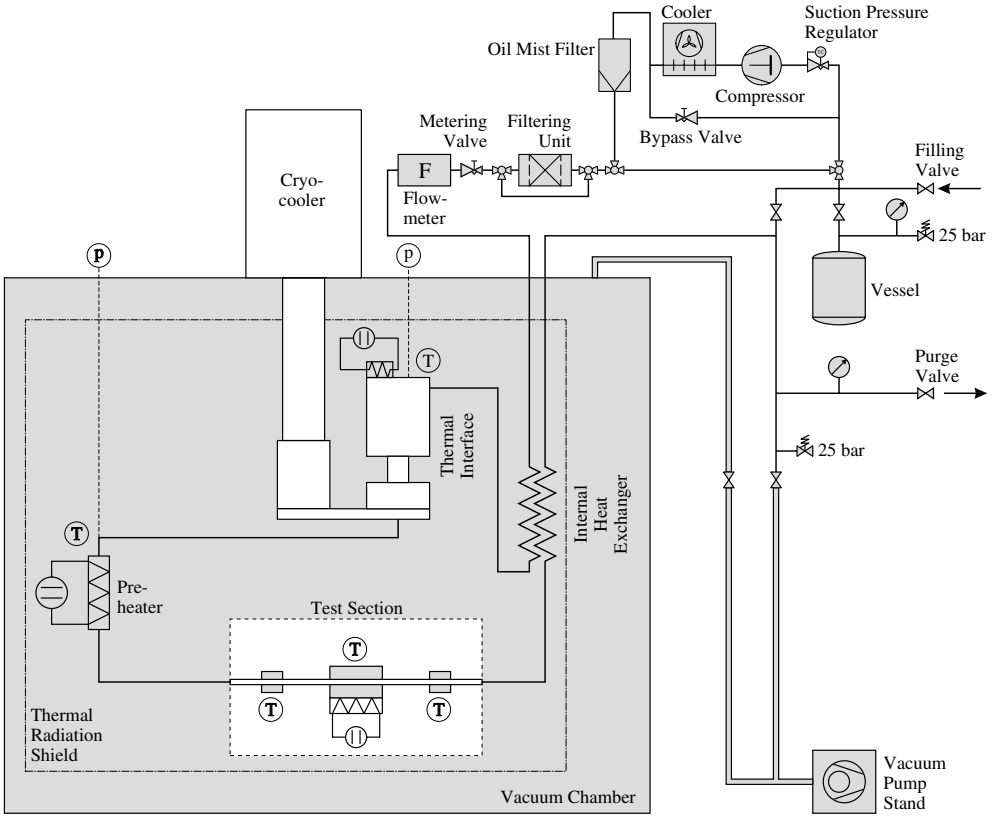

Fig. 2. Experimental set-up for heat transfer measurements in microtubes at cryogenic temperatures.

saturation temperature/pressure was stabilized by a temperature controller, using an electrical heater and a temperature sensor both installed on top of the thermal interface. The pre-heater and the test section were assembled on the same tube, with a tube length before the test section much larger than the hydrodynamic entry length. The (single-phase) fluid temperature or (two-phase) fluid quality at the test section inlet were controlled by the pre-heater power.

The fluid flow rate was controlled by both the bypass and the metering valve, and measured with a thermal flowmeter at ambient temperature. Temperatures in the cold part were measured with PT-100 sensors and a cryogenic temperature monitor. Both the sensors and the electrical heaters were equipped for 4-lead differential measurement, and the leads were heat-sinked to the cryocooler. The strain gauge pressure transducers operated at room-temperature were connected with the cold circuit through capillary tubes. High-impedance filter frits were implemented to damp possible thermoacoustic oscillations.

2.2. Measuring concept

The test section shown in Fig. 3 consisted of three high-conductivity copper blocks, which were soft-soldered onto the microtube. The middle block formed the compound heat exchanger together with the solder tin layer and the tube. It was heated by an electrical heater. The heater and the temperature sensor T_b were connected on opposite sides of the copper body. Two adiabatic copper blocks for temperature measurement were located up- and downstream of the heat exchanger at a distance larger than the thermal fin length in the tube. Since there was no heat load to these two blocks, the measured temperatures T_{in} and T_{out} were identical with the fluid bulk temperatures at these points. The temperature sensors T_{in}, T_b and T_{out} were cross-calibrated.

The mean heat transfer coefficient $\bar{\alpha}$ in such a compound heat exchanger is defined as

$$\bar{\alpha} = \frac{\dot{Q}}{A_w \Delta T_{m,w}}, \tag{1}$$

where $\dot{Q}$ is the heat load, A_w the wetted surface of the flow channel, and $\Delta T_{m,w}$ the mean temperature difference. $\Delta T_{m,w}$ is given in single-phase flow by the logarithmic mean temperature difference

$$\Delta T_{m,w} = \frac{T_{out} - T_{in}}{\ln\left(\frac{\overline{T}_w - T_{in}}{\overline{T}_w - T_{out}}\right)}, \tag{2}$$

and in two-phase flow by

$$\Delta T_{m,w} = \overline{T}_w - \overline{T}_{fl}. \tag{3}$$

T_{in} and T_{out} are the fluid bulk temperatures at the inlet and at the outlet, $\overline{T}_{fl}$ is the mean fluid temperature in the heat exchanger, and $\overline{T}_w$ is the mean temperature of the wetted surface.[3]

As $\overline{T}_w$ could not be measured directly, the copper body temperature T_b was measured, and Eqs. (1)–(3) were changed to

$$\overline{k} = \frac{\dot{Q}}{A_w \Delta T_{m,b}}, \tag{4}$$

with

$$\Delta T_{m,b} = \frac{T_{out} - T_{in}}{\ln\left(\frac{T_b - T_{in}}{T_b - T_{out}}\right)} \tag{5}$$

in single-phase flow, and

$$\Delta T_{m,b} = T_b - \overline{T}_{fl} \tag{6}$$

in two-phase flow.

$\overline{k}$ is the mean *overall* heat transfer coefficient related to the wetted surface A_w, obtained directly from the measured data. The heat exchange between the fluid and the area in the copper body, where the temperature sensor T_b is located, can be modeled as a series connection of thermal resistances R. The measured overall heat transfer coefficient $\overline{k}$ is then expressed in the form

$$\overline{k} = \frac{1}{(\overline{R}_z + R_{eff})A_w}. \tag{7}$$

Here, R_{eff} is defined as the *effective thermal resistance* of the compound heat exchanger, and includes both conductivity and contact resistances of the various layers between the wetted surface A_w and the location of the temperature sensor T_b. If R_{eff} is known, $\bar{\alpha}$ can be calculated as

$$\bar{\alpha} = \frac{\bar{k}}{1 - \bar{k} A_w R_{eff}}. \tag{8}$$

In the experiments, R_{eff} was measured by fitting a model for single-phase turbulent heat transfer to a data set on overall heat transfer coefficients $\bar{k}$. The data set was

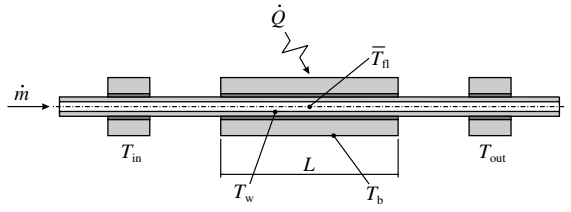

Fig. 3. Layout of the test section, showing the locations of temperature measurement.

[3] Eqs. (2) and (3) are valid as the inner wall temperature was almost constant along the heat exchanger axis z with $\Delta T_w(z) < 1.0$ K, which was achieved by the high conductivity and by the geometry of the heat exchanger's copper body (see [19]).

taken with sub-cooled liquid at varying mass flow, where the heat transfer coefficient mainly depended on Re. The thermal conditions, i.e. the heat load and the fluid temperature level, were kept constant. From the fit one could then extract the varying heat transfer coefficient $\bar{\alpha}$, and some static parameter that involved the difference between $\bar{\alpha}$ and $\bar{k}$ as an extrapolation to infinite Reynolds numbers ($\overline{R}_\alpha \to 0$ at $Re \to \infty$).

The fit function for the experimental data was developed by writing Eq. (7) in the form

$$\frac{1}{\bar{k}} = \frac{1}{\bar{\alpha}} + R_{\text{eff}} A_{\text{w}}, \tag{9}$$

and by substituting $\bar{\alpha}$ with

$$\bar{\alpha} = \frac{Nu\lambda}{d}, \tag{10}$$

and Nu with the Gnielinski equation [6] as heat transfer model for the transition region of $2300 < Re < 10^4$

$$Nu = \text{H0}(Re^{\text{H1}} - \text{H2})Pr^{0.4}\left[1 + \left(\frac{d}{L}\right)^{\frac{2}{3}}\right]K_{\text{T}} \tag{11}$$

(for gases: $\text{H0} = 0.0214$, $\text{H1} = 0.8$, $\text{H2} = 100$, $K_{\text{T}} = 1$; for liquids: $\text{H0} = 0.012$, $\text{H1} = 0.87$, $\text{H2} = 280$, $K_{\text{T}} = (\eta/\eta_{\text{w}})^{0.11}$). H0, H1 and H2 are the parameters of the heat transfer model. The dimensionless numbers Re, Pr and K_{T}, as well as the fluid thermal conductivity λ are the variables determined from the actual mean fluid properties at each data point.

The suitability of this fit function is shown in Section 3.1 together with the experimental results. The measured values of R_{eff} were considered as a constant for each tube in all single- and two-phase experiments. This assumption is discussed in more detail in [19].

2.3. Characteristic dimensions

For the analysis of experimental data and their representation in form of correlations it is essential to determine the characteristic dimensions of the tubes used in the experiments. This is particularly important in the case of microtubes, where the actual diameter may deviate from the nominal diameter, and where the macroscopic surface roughness can have a significant influence on the heat transfer.

In tubes with large roughness, the cross-section A_{c} and the wetted surface A_{w} have to be defined independently. Fig. 4 compares a circular smooth tube of diameter $d = d_{\text{c}}$ with a rough tube of the same cross-sectional area. One characteristic dimension of such a rough tube can be defined as

$$d_{\text{c}} = \sqrt{\frac{4A_{\text{c}}}{\pi}}, \tag{12}$$

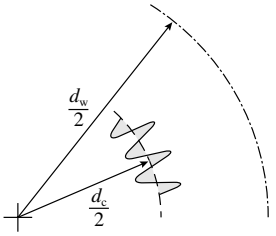

Fig. 4. Characteristic dimensions in rough tubes.

which is the diameter of a perfectly smooth circular tube of the same cross-sectional area. A second characteristic dimension d_{w} shall be defined as

$$d_{\text{w}} = \frac{P}{\pi}. \tag{13}$$

P is the perimeter of the rough tube, and d_{w} is the diameter of a perfectly smooth circular tube with identical wetted surface area. The wetted surface area of a heat exchanger of length L is given as

$$A_{\text{w}} = PL, \tag{14}$$

assuming that the axial roughness is small compared to the radial roughness (which is usual for drawn tubes). A_{c} and therefore d_{c} determine the fluid velocity and the mass flux, while d_{w} is the characteristic dimension for Re and Nu.

The literature review on surface roughness effects in small tubes by Kandlikar et al. [23] shows that the hydraulic diameter

$$d_{\text{h}} = \frac{4A_{\text{c}}}{P} \tag{15}$$

is used almost exclusively as characteristic dimension. However, from Fig. 4 it is evident that d_{h} has no physical relation to the wetted surface of tubes with large roughness. This explains why experimental data of larger tubes are usually in good agreement with theoretical predictions, whereas deviations increase toward small dimensions, i.e. increasing relative roughness. It is also important to note that the actual wetted surface area A_{w} of tubes with large roughness can only be determined by direct optical measurement, and *not* indirectly through d_{h} by means of e.g. pressure drop measurements with laminar flow.

Fig. 5 shows examples of microscope images, from which the two characteristic dimensions d_{c} and d_{w} of the test tubes were determined. After finishing the experiments, three cross-sectional samples were prepared from each microtube, and images with reference dimensions were taken under an electron microscope. The images were converted into vector graphics, which allowed to measure the actual cross-sectional area A_{c} and the perimeter P. The results of the image analysis

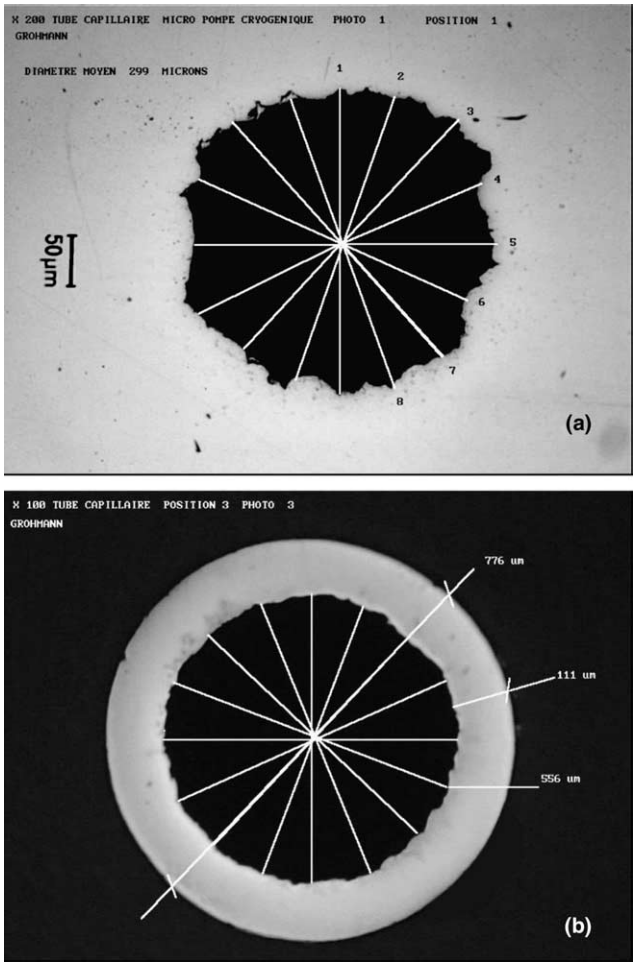

Fig. 5. Example images of transversal cuts through the microtubes. (a) Tube 800 × 250 μm, magnification × 200; (b) tube 800 × 500 μm, magnification × 100.

are summarized in Table 1. The data presented are mean values and their RMS deviation, determined from the values measured for the three cross-sectional images.

The relative roughness of these test tubes can be expressed with a new parameter r_d defined as

$$r_d = \frac{d_w}{d_c}. \tag{16}$$

This parameter has values of

$r_d = 1.20 \pm 0.12$ (250 μm tube),
$r_d = 1.07 \pm 0.02$ (500 μm tube),
$r_d = 1.0$ (smooth tube),

and represents a measure for changed surface to volume ratios compared to smooth circular tubes. It is not identical with the commonly used relative roughness ϵ, which

Table 1
Characteristic dimensions of the microtubes used in the experiments

Microtube (OD × ID)	800 × 250 μm	800 × 500 μm
Perimeter P	$(106.5 \pm 8.1) \times 10^{-5}$ m	$(184.6 \pm 2.5) \times 10^{-5}$ m
Cross-section A_c	$(63.0 \pm 8.8) \times 10^{-9}$ m^2	$(238.4 \pm 4.8) \times 10^{-9}$ m^2
Heat exchanger length L	3.0×10^{-2} m	3.0×10^{-2} m
Wetted surface A_w	$(31.9 \pm 2.4) \times 10^{-6}$ m^2	$(55.4 \pm 0.8) \times 10^{-6}$ m^2
Characteristic dimension d_c	283 ± 20 μm	551 ± 6 μm
Characteristic dimension d_w	339 ± 26 μm	588 ± 8 μm

is defined as $\epsilon = R_a/d$. Here, R_a is the arithmetic mean of the absolute values of vertical deviation from the mean line through the rough profile, and d is the mean line diameter.

The usefulness of r_d will be demonstrated in the modeling of experimental data in Section 3.1.

2.4. Experimental program and data analysis

The scope of the experiments was to study typical cooling conditions of cryogenic tracking detectors. Argon of 99.9995% purity was used as working fluid at a system pressure of $p_s \approx 15$ bar, corresponding to $T_s \approx 124$ K.

In single-phase heat transfer, the experimental program was focused on the measurement of the effective thermal resistance R_{eff}, and on supporting the modeling of flow-boiling heat transfer. The studies were limited to the following:

- *Turbulent liquid flow*: Experiments were performed at constant heat load and variable flow rate with liquid of about 30–15 K sub-cooling. For each tube, the parameters of the heat transfer correlation and R_{eff} were obtained from fitting the same set of data.
- *Turbulent vapor flow*: Experiments and system design were not focused on vapor-phase measurements. However, data were taken to support the modeling of convective boiling heat transfer. The data measured at 5–25 K super-heating were less accurate than the liquid-phase measurements.
- *Laminar liquid flow*: Experiments were conducted at constant heat load and variable flow rate with liquid of about 35–10 K sub-cooling. Mean heat transfer coefficients were measured in hydrodynamically developed flow and at constant wall temperature.
- *Laminar vapor flow*: The system was not designed for this flow regime.

Turbulent liquid data were analyzed first to obtain both the fitted turbulent liquid flow heat transfer correlation, and the effective thermal resistance R_{eff}. The turbulent vapor flow and the laminar liquid flow data, as well as the two-phase data were analyzed afterwards with R_{eff} as a fixed parameter.

Experiments on flow-boiling heat transfer were focused on nucleate boiling, which is the dominant regime in high heat flux electronics cooling. However, a few data were taken under pure convective boiling conditions to support the modeling of experimental results. The experiments included:

- *Convective boiling*: Experiments were performed with a heat flux lower than required for the onset of nucleate boiling ($\dot{q} < \dot{q}_{onb}$). Data series were taken at constant mass flow, constant heat load (constant Δx) and variable inlet quality x_{in}.
- *Flow-boiling*: Experiments were conducted in the nucleate boiling dominated regime at a heat flux $\dot{q} > \dot{q}_{onb}$. Data series were taken at constant mass flow rates. Mean heat transfer coefficients along the tube length L were measured, i.e. for a quality range between $x_{in} \approx 0$ and x_{out}. The heat load $\dot{Q}$ was ramped up until the outlet quality reached $x_{out} \approx 1$, or until critical boiling conditions occurred.

Generally, local heat transfer coefficients cannot be measured directly in two-phase flow, as the heat load implies a quality change Δx. The concept was therefore to measure mean heat transfer coefficients $\bar{\alpha}$ between $x_{in} \approx 0$ and x_{out}, and to fit the experimental data with a heat exchanger model that numerically integrated correlated local heat transfer coefficients. The modeling of the local flow-boiling heat transfer was based on the *VDI Wärmeatlas* correlation edited by Steiner [24]. The C++ fitting algorithms for both the single-phase and the two-phase data are explained in [19].

3. Results

Detailed values for each data point presented in this Section, including error margins, are published in [19].

3.1. Single-phase turbulent liquid flow

The experimental results for single-phase turbulent liquid flow are shown in Fig. 6. The quality of the fits proves that both the turbulent heat transfer model and the concept of measuring the effective thermal resistance R_{eff} are appropriate.

The results of the fits are summarized in Table 2. The coefficients H0 and H2 were fixed to the values given by Eq. (11). H1 was chosen as a free parameter in a first fit, and then fixed to the fitted value in a second fit to obtain the error of R_{eff}.

The effective thermal resistance was mainly determined by the conductivity resistances of the stainless steel tubes and the solder tin layers, as well as by the contact resistances. R_{eff} was therefore larger for the 800×250 μm tube. The influence of R_{eff} on $\bar{k}$ in Eq. (7) increased with the heat transfer coefficient $\bar{\alpha}$, and ranged for all measured data from $R_{eff}/\overline{R}_\alpha = 0.01$ in single-phase laminar flow to $R_{eff}/\overline{R}_\alpha = 0.94$ during nucleate boiling at the highest heat flux.

The heat transfer coefficients are plotted together with the conventional correlation of Eq. (11) in Fig. 7. The results are similar to the data published by Adams et al. [3]. With respect to the conventional correlation, the heat transfer is obviously enhanced with decreasing diameter, which is also seen at the fitted *Re*-exponents H1 in Table 2.

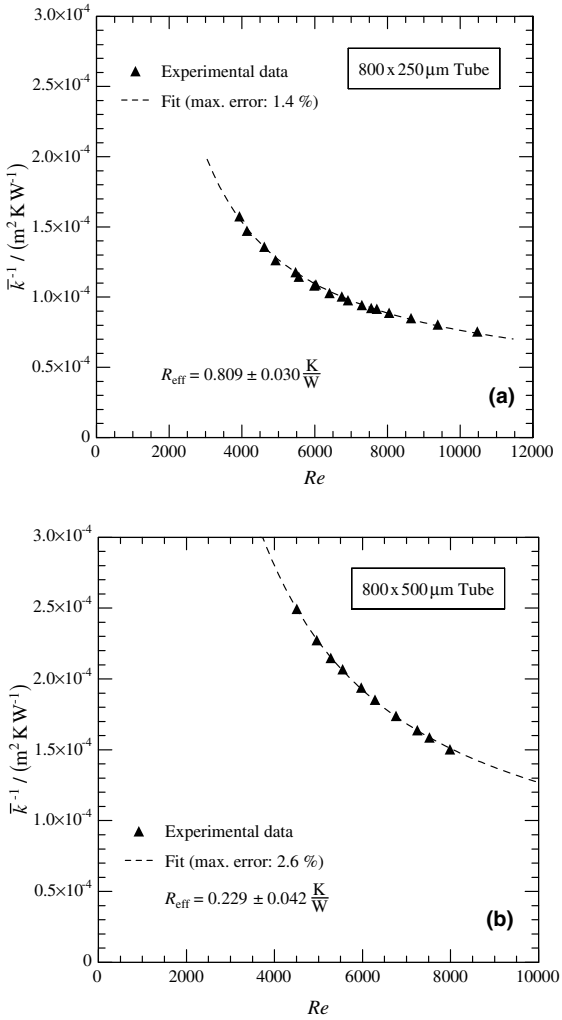

Fig. 6. Results of fitting turbulent liquid flow heat transfer data with Eq. (9).

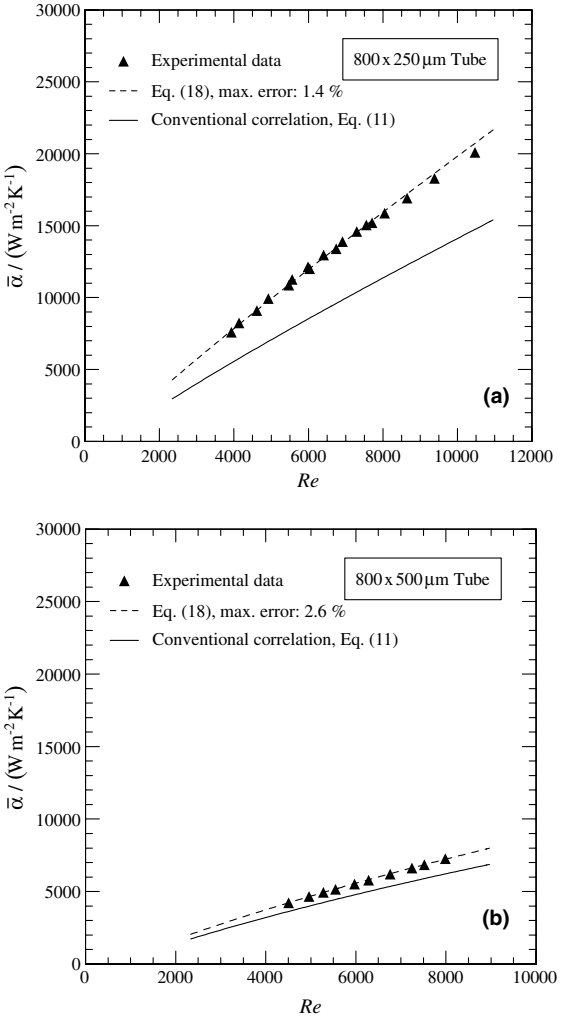

Fig. 7. Heat transfer coefficients in single-phase turbulent liquid flow.

However, the experimental results for both tubes can be modeled with *one* equation, if the relative roughness parameter r_d defined in Eq. (16) is implemented in the *Re*-exponent H1 in the form of

$$H1 = H1_{smooth} \cdot r_d^n. \quad (17)$$

The fit of the coefficient n with the data from both tubes then yields

Table 2
Fitted parameters in single-phase turbulent liquid flow

Fit function	800×250 µm tube	800×500 µm tube
	$\frac{1}{\bar{k}} = \frac{d_w}{H0(Re^{H1} - H2)Pr^{0.4}\left[1 + \left(\frac{d_w}{L}\right)^{\frac{2}{3}}\right]\left(\frac{\eta}{\eta_w}\right)^{0.11}\lambda} + H3A_w$	
H0 (fixed)	0.012	
H1	0.904	0.885
H2 (fixed)	280	
H3 (R_{eff})	0.809 ± 0.030 K/W	0.229 ± 0.042 K/W

$$Nu_{\mathrm{turb,l}} = 0.012[Re^{(0.87 \cdot r_{\mathrm{d}}^{0.22})} - 280] \cdot Pr^{0.4}\left[1 + \left(\frac{d_{\mathrm{w}}}{L}\right)^{\frac{2}{3}}\right] \cdot \left(\frac{\eta}{\eta_{\mathrm{w}}}\right)^{0.11}. \quad (18)$$

The maximum error between the measured data and Eq. (18) is 1.4% and 2.6%, respectively. One can therefore conclude that the enhancement of heat transfer is only due to the relative roughness r_{d}, and not due to a diameter dependence specific to microtube dimensions. Eq. (17) is fully consistent with the turbulent heat transfer correlation of Eq. (11) for *smooth* circular tubes.

3.2. Single-phase turbulent vapor flow

The measured turbulent heat transfer coefficients in the vapor phase are shown in Fig. 8. The trend in Fig. 8b shows similar behavior as the liquid phase data. The results for the 250 μm tube, however, do not follow the trend of the correlation at high *Re*, which is due to systematic errors (large pressure drops) in the experimental set-up at these conditions.

As there is no fundamental difference between liquid and vapor phase heat transfer, only the experimental data of the 500 μm tube were fitted with the type of Eq. (18), yielding

$$Nu_{\mathrm{turb,v}} = 0.0214[Re^{(0.8 \cdot r_{\mathrm{d}}^{0.55})} - 100] \cdot Pr^{0.4}\left[1 + \left(\frac{d_{\mathrm{w}}}{L}\right)^{\frac{2}{3}}\right]. \quad (19)$$

Eq. (19) matches the low-*Re* data in Fig. 8a, where the pressure drop was less significant. The correlation is consistent with the conventional correlation Eq. (11) for turbulent vapor heat transfer in smooth circular tubes. However, more statistics of dedicated vapor phase experiments is required to generally validate Eq. (19).

3.3. Single-phase laminar liquid flow

The experimental results for laminar liquid flow are shown in Fig. 9. At low *Re*, the data fit well with $Nu_{\infty} = 3.656$ for fully developed flow. In the entry region, however, the heat transfer is superior to the conventional correlation. This is explained with the breakage of the boundary layers at the surface asperities.

The results of the fits are summarized in Table 3. Unlike in turbulent flow, the data cannot yet be modeled with one correlation.

Measured and modeled mean heat transfer coefficients $\bar{\alpha}$ are shown in Fig. 10 as a function of *Re*. The trend of a good agreement between data and conventional correlation at low *Re*, and increasing positive deviations with increasing *Re*, is similar to the data published by Rahman [2].

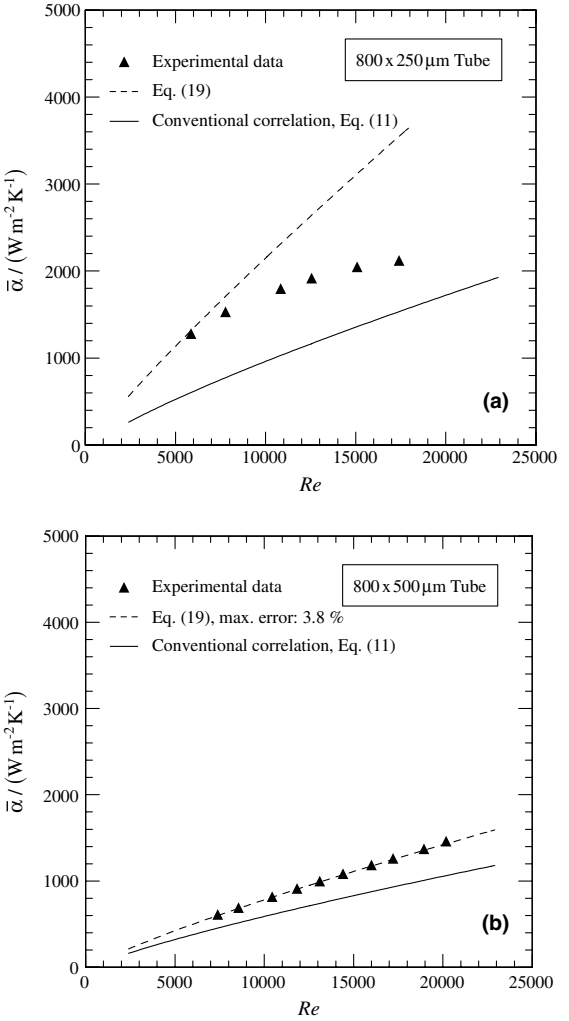

Fig. 8. Heat transfer coefficients in single-phase turbulent vapor flow.

The flow transition to turbulent flow can be clearly identified in Fig. 10a, with $Re_{\mathrm{crit}} = 1575 \ll 2300$. Unfortunately, the flow transition could not be measured in the 500 μm tube, as the experimental set-up could not be operated with higher flow rates under these conditions.

3.4. Flow-boiling/convective boiling

In the *VDI Wärmeatlas* correlation [24], the local flow-boiling heat transfer coefficient α is defined as a function of the convective boiling heat transfer coefficient α_{c} and the nucleate boiling heat transfer coefficient α_{nb}:

$$\alpha = \sqrt[3]{\alpha_{\mathrm{c}}^3 + \alpha_{\mathrm{nb}}^3}. \quad (20)$$

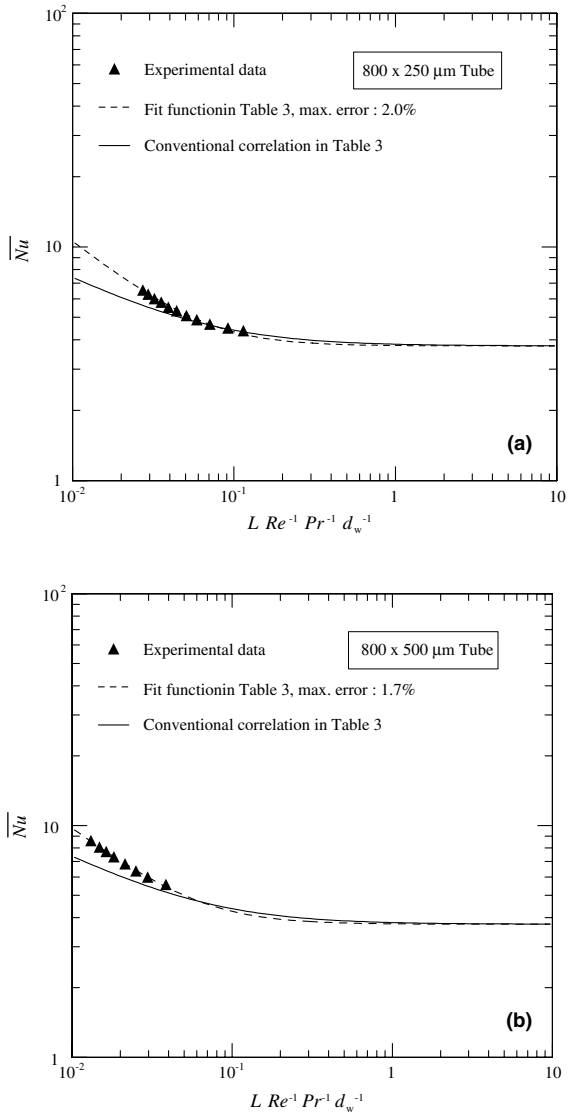

Fig. 9. Nusselt numbers in single-phase laminar liquid flow.

If nucleate boiling occurs, it usually dominates the flow-boiling heat transfer.

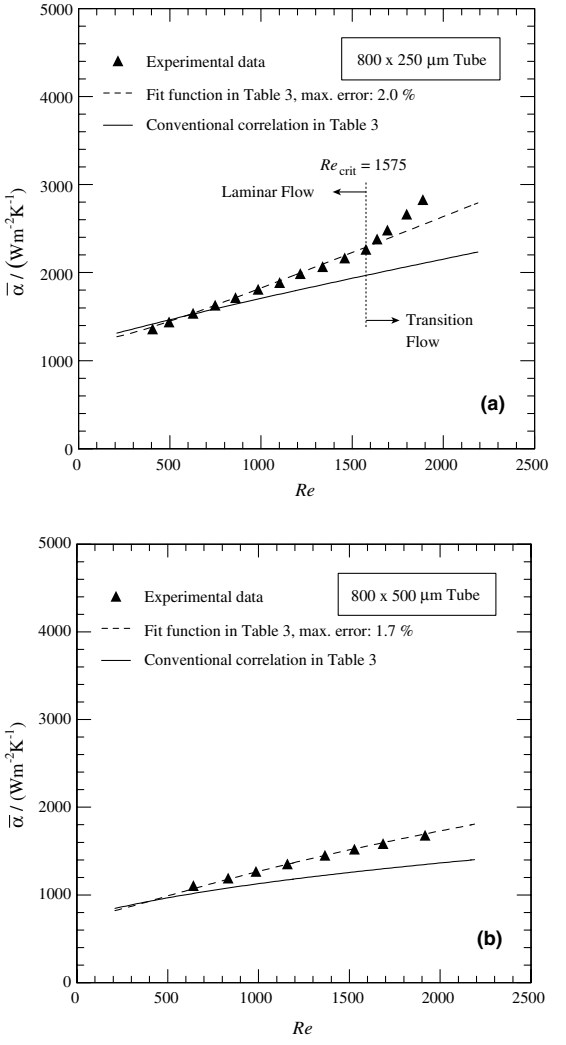

Fig. 10. Heat transfer coefficients in single-phase laminar liquid flow.

Convective boiling conditions appear at low heat flux, where the wall superheat is too small for the activation of nucleation centers, and where the evaporation takes place at the liquid/vapor phase boundary. Convec-

Table 3
Fitted parameters in single-phase laminar liquid flow

	800×250 µm tube	800×500 µm tube
Fit function	$\overline{Nu}_{\mathrm{lam},l} = \left[\left(\frac{a}{1-n}\left(\frac{RePrd_w}{L}\right)^n\right)^3 + Nu_\infty^3\right]^{\frac{1}{3}}\left(\frac{\eta}{\eta_w}\right)^{0.14}$	
a	0.391	0.421
n	0.538	0.515
Nu_∞ (fixed)	3.656	

Conventional correlation: $a = 0.89$, $n = 0.35$, $v_\infty = 3.656$.

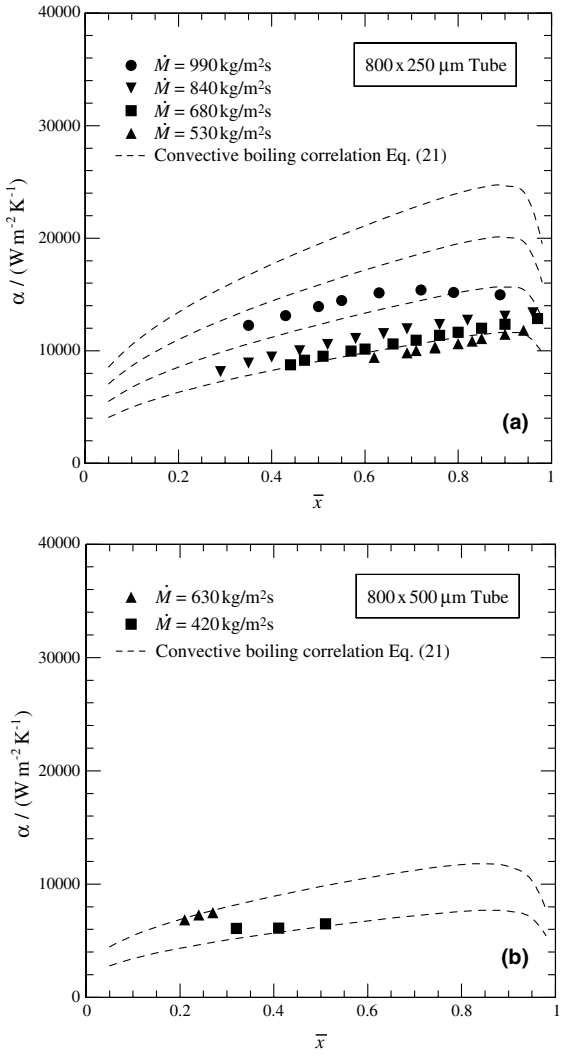

Fig. 11. Results of convective boiling heat transfer measurements.

tive boiling heat transfer depends mainly on the mass flux $\dot{M}$, the quality x, and the density ratio ρ_l/ρ_v. The *VDI Wärmeatlas* correlation [24] for convective boiling in vertical tubes is given by Eq. (21), where $\alpha_{l,0}$ and $\alpha_{v,0}$ are the local single-phase heat transfer coefficients for the condition that the fluid was flowing at the same mass flux in form of saturated liquid and saturated vapor, respectively.

Although convective boiling plays a minor role in most flow-boiling heat transfer conditions under high heat flux, the experimental data summarized in Fig. 11 were taken to verify Eq. (21). The results for the 500 µm tube in Fig. 11b were in very good agreement, using Eqs. (18) and (19) to determine the single-phase heat transfer coefficients $\alpha_{l,0}$ and $\alpha_{v,0}$. In the 250 µm tube, the agreement between experiment and correlation was within 10% for the data series of $\dot{M} = 530\ \mathrm{kg/m^2\,s}$. At higher mass flux, however, the correlation over-predicted the experimental data by up to 60%. Nevertheless, Eq. (21) was used unchanged in Eq. (20) to model the flow-boiling heat transfer data presented hereafter.

$$\frac{\alpha_c}{\alpha_{l,0}} = \left\{ (1-x)^{0.01}\left[(1-x)^{1.5} + 1.9x^{0.6}\left(\frac{\rho_l}{\rho_v}\right)^{0.35}\right]^{-2.2} + x^{0.01}\left[\frac{\alpha_{v,0}}{\alpha_{l,0}}\left(1 + 8(1-x)^{0.7}\left(\frac{\rho_l}{\rho_v}\right)^{0.67}\right)\right]^{-2}\right\}^{-0.5} \tag{21}$$

3.5. Nucleate boiling

In the nucleate boiling experiments, the fluid was always entering the test section slightly sub-cooled with $x_{in} \approx -0.05$.[4] A heat flux $\dot{q} \geqslant \dot{q}_{onb}$ was then needed to generate two-phase flow. At the lower limit of $\dot{q}$, experiments were conducted with a heat flux just high enough for stable two-phase operation. This was usually obtained at outlet qualities of $x_{out} =$ 0.10–0.20. The start of dryout was seen in the data series of mean heat transfer coefficients, when data points of higher heat flux fell below the *trend* of lower heat flux data.

The measured temperature differences as a function of the heat load are plotted in Fig. 12 for all experiments carried out in the nucleate boiling dominated regime. The data were correlated with the nucleate boiling heat transfer model for vertical tubes in [24], which has the general form of

$$\frac{\alpha_{nb}}{\alpha_0} = C_F\left(\frac{\dot{q}}{\dot{q}_0}\right)^n F(p^\star)F(d)F(W)\,F(\dot{M},x). \tag{22}$$

α_0 is the reference heat transfer coefficient in pool boiling at the heat flux $\dot{q}_0$. For argon these values are

$$\alpha_0 = 3870\ \mathrm{W/m^2\,K}, \quad \text{at}$$
$$\dot{q}_0 = 10\,000\ \mathrm{W/m^2}.$$

The fluid properties are considered by the factor C_F, wall properties by a factor $F(W)$, tube dimensions by a factor $F(d)$ and flow conditions by a factor $F(\dot{M},x)$. The influence of the saturation pressure is included in $F(p^\star)$, and the heat flux dependence is described by the power function $(\dot{q}/\dot{q}_0)^n$.

3.5.1. Flow- and heat transfer regimes

A systematic influence of flow regimes on flow-boiling heat transfer is only confirmed for horizontal tubes, and operating conditions with significant phase separation

[4] The negative vapor fraction shall indicate the amount of sub-cooling, in terms of $x_{in} = (h_{in} - h')/(h'' - h')$.

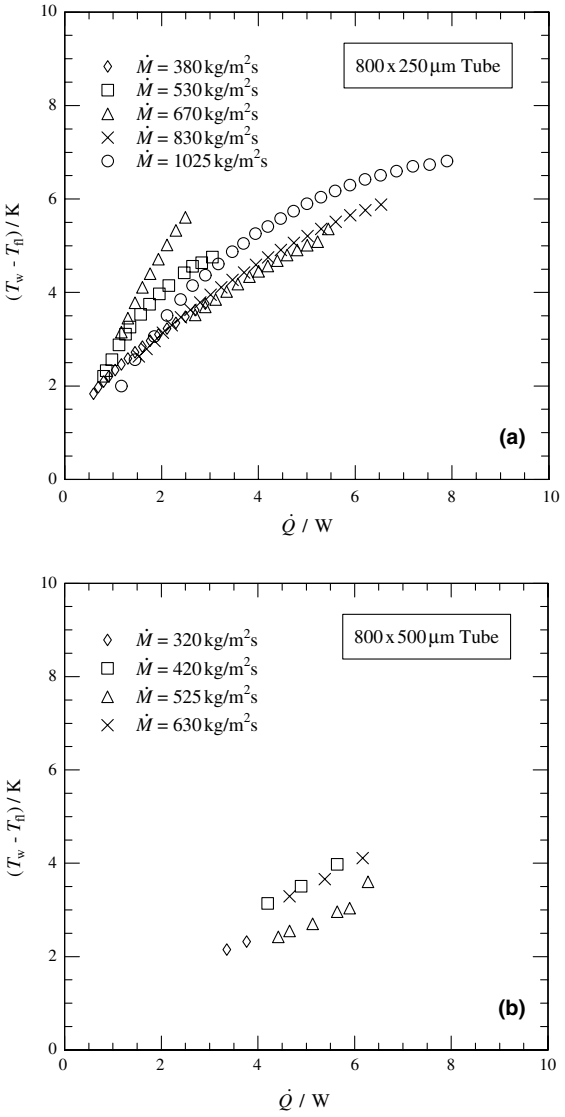

Fig. 12. Summary of measured temperature differences in nucleate boiling.

and partial surface dryout. Such conditions are unlikely to occur in microtubes, and flow patterns were therefore not studied in detail.

However, the flow regime can still have a significant influence on the heat transfer, which is shown in Fig. 13. The data points represent mean heat transfer coefficients $\bar{\alpha}$ between $x_{in} = -0.05$ and x_{out}, taken at a constant mass flow and with a step-wise increase of the heat load. At $x_{out} = 0.44$, the mean heat transfer coefficient increased by 70% at just a slight increase of the heat flux ($\Delta\dot{q} = 8\%$) and the outlet quality ($\Delta x_{out} = 5\%$). Such a step in the *mean* heat transfer coefficient can only be explained, if the *entire* flow and heat transfer regime in the heat exchanger changed. This strong change can

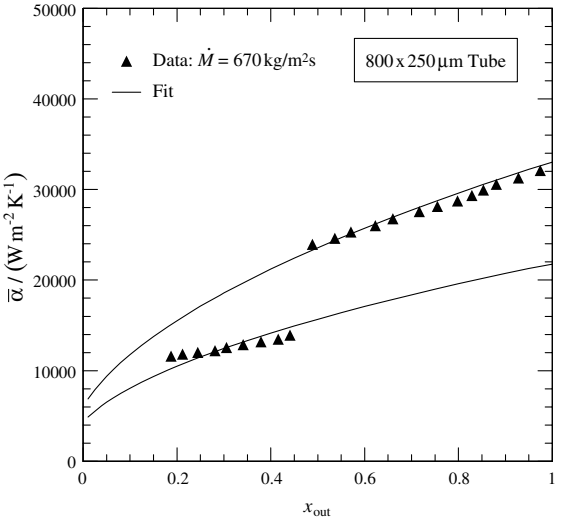

Fig. 13. Variation of flow and heat transfer regimes in two-phase flow.

neither be explained by the heat flux dependence $\bar{\alpha} = f(\dot{q})$ (which is already given by the slope of the data), nor by the local quality dependence $\alpha_z = f(x_z)$, which would only influence a small fraction at the outlet. A consequence is then that two-phase flow regimes can be meta-stable. They do not only depend on local conditions (which in Fig. 13 have hardly changed in large parts of the heat exchanger between the data points of $x_{out} = 0.44$ and 0.49), but can be influenced by retroactive effects and by the history of the flow.

Although not proven optically in the experiments, one can imagine that such meta-stable flow regimes are associated with the number of active nucleation centers, which is not necessarily always the same under reproduced operating conditions. Flow-boiling heat transfer correlations therefore have rather large uncertainties. The standard deviation between the correlation and data from an experimental database is given in [24] for a number of fluids, ranging from ±4% to ±96%. High statistics is consequently required to understand the difference between intrinsic heat transfer variations, and systematic effects that can be modeled.

3.5.2. Heat flux and mass flux dependence

Although the test tubes were installed in horizontal orientation, the fit of the experimental data in Fig. 14 shows that there was no mass flux and quality dependence in these microtubes.[5] This is explained by a stronger influence of the surface tension in microtubes, which makes phase separation phenomena less likely to occur.

[5] The differences between the two data series are only due to higher heat fluxes at higher flow rates.

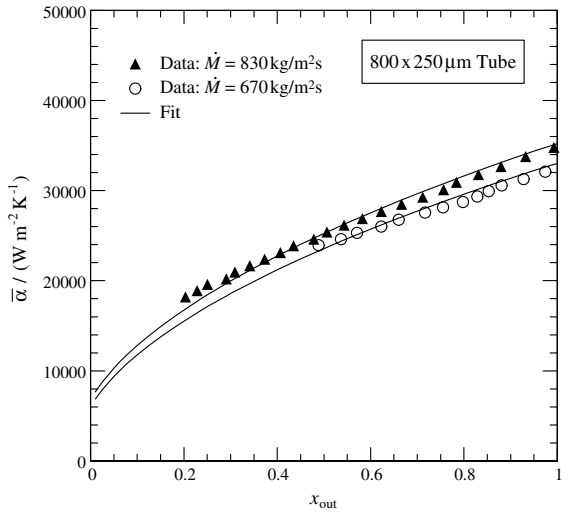

Fig. 14. Heat flux and mass flux dependence of mean heat transfer coefficients.

As the tube orientation obviously had no significant influence on the nucleate boiling heat transfer, the modeling of α_{nb} was based on the *VDI Wärmeatlas* correlation for *vertical* tubes (Eq. (22)). Here, the heat flux exponent n is a function of the reduced pressure, and yields for cryogenic fluids:

$$n = 0.7\text{–}0.13 \times 10^{0.48p^\star}. \tag{23}$$

The factor $F(\dot{M},x)$ is

$$F(\dot{M},x) = 1. \tag{24}$$

All the experimental data presented in this Section were fitted with these n and $F(\dot{M},x)$ as constants. The excellent agreement between the data points and the fit in Fig. 14 proves that the heat flux dependence is well described with Eq. (23).

3.5.3. Saturation pressure dependence

The influence of the saturation pressure in Eq. (22) is described in [24] by the function

$$F(p^\star) = 2.816p^{\star 0.45} + \left(3.4 + \frac{1.7}{1-p^{\star 7}}\right)p^{\star 3.7}, \tag{25}$$

where $p^\star = p_s/p_c$ is the reduced pressure. As fluid properties are independent of scaling, the function was used without modification.

3.5.4. Influence of wall properties

Although the effect of surface properties is not known in detail, the influence of roughness in Eq. (22) is taken into account in [24] by the function

$$F(W) = \left(\frac{R_a}{R_{a,0}}\right)^{0.133}, \tag{26}$$

with $R_{a,0} = 1$ µm. From the microscope images, the arithmetic mean roughness R_a of the microtubes was estimated as

$$R_a = 9\ \mu\text{m} \quad (800 \times 250\ \mu\text{m tube}),$$
$$R_a = 7\ \mu\text{m} \quad (800 \times 500\ \mu\text{m tube}),$$

yielding factors of $F(W) = 1.34$ and $F(W) = 1.30$, respectively.

3.5.5. Diameter dependence

The factor $F(d)$ in Eq. (22), [24] describes the increase of heat transfer at decreasing diameter:

$$F(d) = \left(\frac{d_0}{d}\right)^{0.4}, \tag{27}$$

with $d_0 = 0.01$ m. This effect can be explained by the increasing surface to volume ratio in small tubes. The application of the characteristic dimensions of *rough* tubes then yields

$$F(d) = \left(\frac{d_0 r_d}{d_c}\right)^{0.4}. \tag{28}$$

Fitting all experimental data of Fig. 12 with Eqs. (22)–(26) and (28), while keeping only C_F^* a free parameter yields values of $C_F^* = 0.16 \pm 0.03$ for the 250 µm tube, and $C_F^* = 0.33 \pm 0.05$ for the 500 µm tube. These results, however, contradict the trend of $F(d)$, and fall below the fluid-specific constant for argon given in [24] as $C_F^* = 0.93 \pm 0.34$.

In [19] it was shown that there is no physical (space) limit for nucleate boiling in microtubes, which is coherent with the observations made by Zhang [13]. One may therefore conclude that the confinement of *bubble growth* is a limiting factor for the heat transfer during nucleate boiling, rather than the amount of superheating or the bubble formation itself.

To model this effect, an extension of $F(d)$ with a so-called *saturation function* of the form

$$F_b = 1 - e^{-c\frac{d_c}{\mathscr{L}}} \tag{29}$$

is proposed, where $\mathscr{L}$ is the Laplace constant

$$\mathscr{L} = \sqrt{\frac{\sigma}{g(\rho_l - \rho_v)}}. \tag{30}$$

The exponential function F_b with the ratio $d_c/\mathscr{L}$ related to the tube and the bubble volume can take values between 0 and 1, if the coefficient c is positive. Fitting all experimental data with this expression while fixing C_F to 0.93 (for argon) yields a diameter dependence of

$$F(d) = \left(\frac{d_0 r_d}{d_c}\right)^{0.4} \cdot \left(1 - e^{-0.45\frac{d_c}{\mathscr{L}}}\right). \tag{31}$$

The individual terms of Eq. (31) are shown graphically in Fig. 15. It is evident that the classical definition of the diameter dependence with Eq. (27) is inappropriate, as

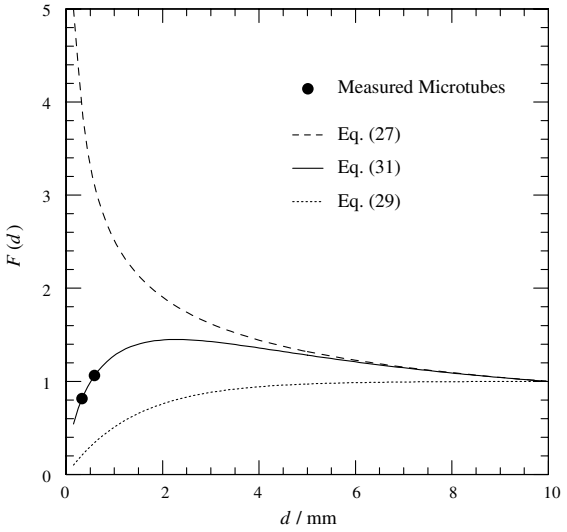

Fig. 15. Diameter dependence $F(d)$ for smooth circular tubes ($r_d = 1.0$) according to Eq. (31).

$(d_0/d)^{0.4}$ becomes infinite in very small tubes. On the other hand, the new factor F_b only becomes effective at tube diameters of $d < 3$ mm, which is consistent with the scope of the conventional correlation in [24].

Fitting all 112 data points of Fig. 12 with Eqs. (22)–(26) and (31), and with the free fluid-specific parameter C_F yields

$$C_F = 0.91 \pm 0.01. \tag{32}$$

The result indicates that 68% of the data fall within the error margin of $C_F = 0.91 \pm 0.01$. This precision, however, can not obscure the fact that the overall accuracy of flow-boiling heat transfer correlations is no better than ±30% to ±40%. This is a consequence of meta-stable flow regimes and unpredictable numbers of active nucleation centers.

3.6. Critical boiling conditions

Film boiling is usually understood as a critical boiling condition that occurs at low quality and high heat flux. However, film boiling can also set in as a result of local dryout. This is shown in Fig. 16 for dry evaporation ($x_{out} \approx 1$) and partial evaporation ($x_{out} < 1$).

In both cases, a slight increase of the heat load $\dot{Q}$ led to thermal runaway of the block temperature T_b. However, the fluid was still entering the heat exchanger slightly sub-cooled at $x_{in} \approx -0.05$. Under normal conditions, the mean heat transfer coefficient could not change so dramatically at just a small increase of the outlet quality. Consequently, the local increase of the wall temperature at the outlet must have been responsible for the onset of film boiling. This condition requires

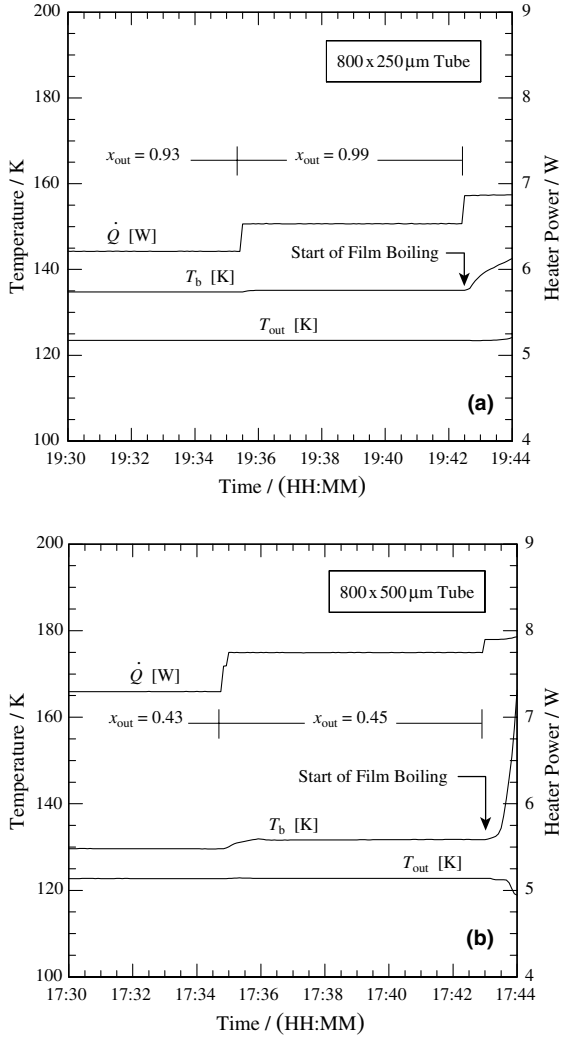

Fig. 16. Film boiling at high quality.

a heat source with no temperature limit, and a high conductivity material to propagate the high wall temperature *upstream* from the outlet (the location of dryout) to the inlet of the heat exchanger. The increased wall temperature signifies a local heat flux $\dot{q}^* > \dot{q}_{crit}$, and causes the liquid film to peel off the wall despite the fact that the nominal heat flux $\dot{q} = \dot{Q}/A_w$ is smaller than $\dot{q}_{crit}$.

Similar results as shown in Fig. 16 were reported by Jiang et al. [17], who defined the critical heat flux (CHF) as the heat flux observed at $x_{out} = 1.0$, where thermal runaway occurred. This CHF, however, is certainly not identical to the critical heat flux $\dot{q}_{crit}$ for film boiling. In our experiments, thermal runaway was observed at the end of *all* data series, at all different mass and heat fluxes. The effect is therefore clearly related to dryout.

Both constructional prerequisites for high-quality film boiling, i.e. an electrical heat source and a high wall conductivity, are present in electronic devices made of silicon. It is therefore essential to avoid any form of dry-out. This can be assured by a sufficient circulation rate of the coolant with e.g. $x_{out} \leqslant 0.5$, and by a reasonable heat flux.

3.7. Stability of flow-boiling

Stability tests of two-phase cooling were carried out with a detector module similar to the module shown in Fig. 1, considering that several authors have observed unsteady flow in parallel microchannels [7,15]. The instabilities were reported to originate from the clogging of individual flow channels with growing vapor bubbles, and the resulting pressure waves then led to flow reversal through a low-impedance by-pass (a parallel channel). Such instabilities, however, will not appear in microtube heat exchangers with a single flow path.

Nevertheless, certain operating conditions close to the boiling line are prone to instabilities. This is demonstrated in Fig. 17a, where the fluid was entering the module slightly sub-cooled ($x_{in} = -0.04$) with a mass flux of $\dot{M} = 140$ kg/m^2 s. The heat load of $\dot{Q} = 1.5$ W was too small to ensure stable nucleation, and the system was therefore permanently oscillating between sub-cooled liquid cooling, liquid superheating, and evaporation.

With an appropriate design, however, microtube cooling systems can be operated in the nucleate boiling regime with a very high stability. Fig. 17b shows the thermal response of the cold detector module, where the nominal heat load for 6 APV25 (1.78 W) was switched on after 6 min. The fluid was entering the module with a quality of $x_{in} = 0.39$ and a mass flux of $\dot{M} = 240$ kg/m^2 s. The temperature stability over a period of 1 h was better than 20 mK, and the stability of the flow was better than the noise of the flowmeter.

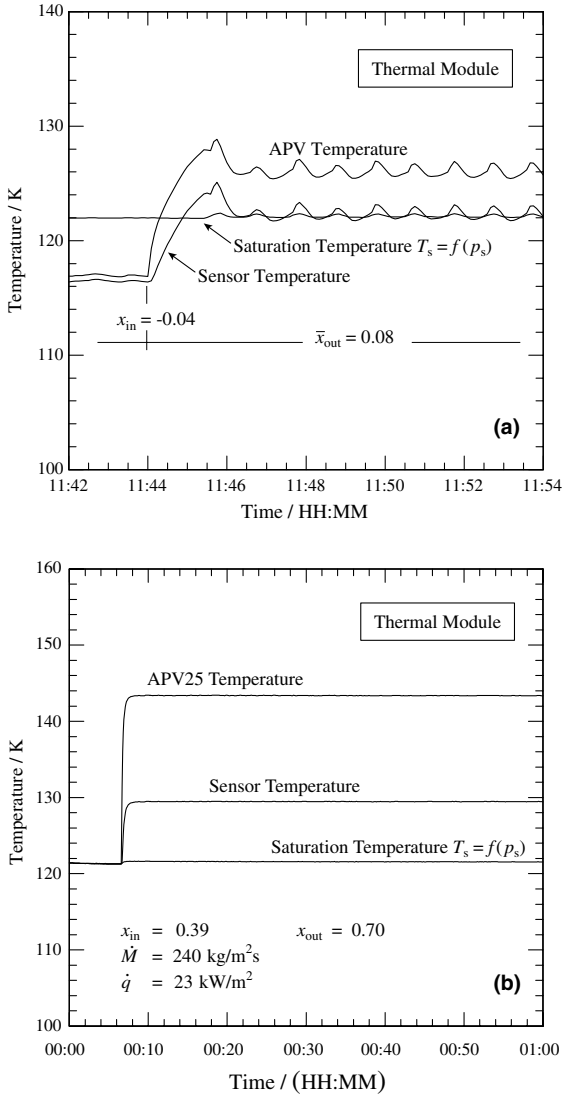

Fig. 17. (a) Instable operation close to the boiling line and (b) stable two-phase cooling.

4. Design of miniature evaporator heat exchangers

The following design rules for miniature evaporator heat exchangers can be deduced from the experimental results:

- The most important design criterion is the heat flux. Too low heat fluxes can cause instabilities in the transition from single- to two-phase flow. Too high heat fluxes can cause critical boiling conditions. The heat flux is the most influential parameter on the heat transfer coefficient.
- The heat flux to provoke nucleate boiling in (nearly saturated) single-phase flow can be considerably higher than the heat flux $\dot{q}_{onb}$ to cause and maintain nucleate boiling in the presence of the two phases. A possibility to achieve stable operation at low quality and low heat flux is J–T expansion into the two-phase area at the heat exchanger inlet.
- Dryout conditions in evaporator heat exchangers must be avoided, choosing a sufficient fluid circulation rate and a reasonable heat flux. Electrical heat sources should always be thermally interlocked to prevent critical boiling conditions and thermal runaway.
- The mass flux and the quality have little or no influence on nucleate boiling heat transfer. High fluid velocities do not improve the heat exchange, which is in contrast to single-phase flow. However, the

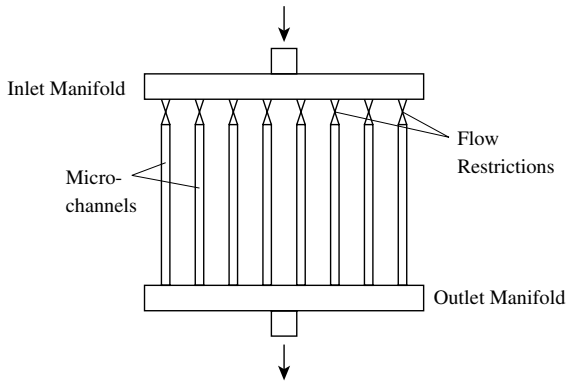

Fig. 18. Evaporator heat exchanger design with parallel microchannels.

stability of systems is usually improved with the (increasing) pressure drop.

- From the last point it follows, with respect to the heat transfer, that short evaporators with a larger diameter are better than long evaporators with a smaller diameter at the same heat exchanger surface. Moreover, circular tubes should be used during nucleate boiling, yielding the lowest pressure drop for a given heat exchanger surface.[6,7]
- Heat exchangers with parallel microchannels should be avoided in nucleate boiling heat transfer, unless instabilities caused by the bubble growth and subsequent flow reversal through a low-impedance bypass are prevented by appropriated means. In addition, the maldistribution of liquid in parallel channels increases the risk of local dryout, which can cause film boiling.

A possible solution to prevent flow instabilities during nucleate boiling in heat exchangers with parallel microchannels is shown in Fig. 18. The heat exchanger is designed in such a way that the flow impedance at the inlet of each microchannel is much larger than at the outlet. This can be achieved by a flow restriction between the inlet manifold and each microchannel, which at the same time can serve as a J–T expansion device. Alternatively, the flow restriction could be designed as a wick, using capillary forces to equally distribute the liquid over the microchannels.

[6] This is in contrast to convective heat transfer (single- or two-phase), where flat channels improve the heat transfer due to the larger surface-to-volume ratio.

[7] The pressure drop in the heat exchanger, however, should be sufficient with regard to stability. The design depends on the overall system layout.

5. Conclusions

Experiments on single-phase and flow-boiling heat transfer in horizontal microtubes of 250 and 500 μm nominal inner diameter were carried out with argon at around 120 K. An experimental technique for heat transfer measurements in microtubes was presented, where the external surface temperature of a compound heat exchanger was measured instead of the temperature of the wetted surface, and where the effective thermal resistance between the wetted and the external surface was determined.

The results on single-phase heat transfer revealed that there is no physical difference in heat transfer mechanisms between macrotubes and microtubes. The enhancement of heat transfer coefficients in small tubes compared to conventional correlations was explained with the increased influence of surface roughness. The effect was modeled with the newly defined relative roughness parameter, yielding Eq. (18) in turbulent liquid flow, and Eq. (19) in turbulent vapor flow.

Flow-boiling experiments focused on the nucleate boiling regime. The results showed no significant influence of the mass flux and the quality. The *VDI Wärmeatlas* correlation for *vertical* tubes (Eq. (22)) was in good agreement with the data, except for the diameter dependence. An extension of the diameter function was therefore proposed in Eq. (31). The measured heat transfer coefficients in the 250 and the 500 μm tube fell below the values in larger tubes under comparable operating conditions.

The phenomenon of high-quality film boiling was described, where the liquid film peeled off the wall starting from the location of dryout. This critical boiling condition requires an electrical heat source, and a high conductivity wall to propagate an increased wall temperature (that signifies an *actual* heat flux beyond the critical heat flux) from the location of dryout *upstream* through the heat exchanger.

Nucleate boiling flow regimes were found to be metastable. The effect was explained with the number of active nucleation centers, which is influenced by the history of the flow. The prediction of nucleate boiling heat transfer coefficients can therefore be no better than about ±30% to ±40%.

It was shown that evaporative microtube cooling systems can be operated with a very high stability. General design rules for microtube evaporator heat exchangers were presented.

Acknowledgements

The author wishes to express his gratitude to Hans Quack (Technische Universität Dresden) and to Tapio Niinikoski (CERN) for supervising the project, and to

Ralf Herzog and Eberhard Wobst (Institut für Luft- und Kältetechnik Dresden) for their support and the funding provided by the German Ministry of Education and Research (BMBF) under the project number 05 ESOXL1. Thanks also go to Blanca Perea Solano, Thomas Eisel and Georg Nüßle for participating in the experiments.

References

[1] W. Qu, G.M. Mala, D. Li, Heat transfer for water flow in trapezoidal silicon microchannels, Int. J. Heat Mass Transfer 43 (2000) 3925–3936.
[2] M.M. Rahman, Measurements of heat transfer in microchannel heat sinks, Int. J. Heat Mass Transfer 27 (4) (2000) 495–506.
[3] T.M. Adams, S.I. Abdel-Khalik, S.M. Jeter, Z.H. Qureshi, An experimental investigation of single-phase forced convection in microchannels, Int. J. Heat Mass Transfer 41 (6–7) (1998) 851–857.
[4] T.M. Adams, M.F. Dowling, S.I. Abdel-Khalik, S.M. Jeter, Applicability of traditional turbulent single-phase forced convection correlations to non-circular microchannels, Int. J. Heat Mass Transfer 42 (1999) 4411–4415.
[5] D. Yu, R. Warrington, R. Barron, T. Ameel, An experimental investigation of fluid flow and heat transfer in microtubes, in: Proceedings of the ASME/JSME Thermal Engineering Conference, vol. 1, 1995, pp. 523–530.
[6] V. Gnielinski, Neue Gleichungen für den Wärme- und Stoffübergang in turbulent durchströmten Rohren und Kanälen, Forschung Ingenieurwesen 41 (1) (1975) 8–16.
[7] S.G. Kandlikar, Two-phase flow patterns, pressure drop and heat transfer during boiling in minichannel and microchannel flow passages of compact evaporators, in: Proceedings of the Third International Conference on Compact Heat Exchangers and Enhancement Technology for the Process Industries, Davos, Switzerland, 2001.
[8] S.G. Kandlikar (Ed.), Proceedings of the 1st International Conference on Microchannels and MinASME, ASME, Rochester, NY, 2003.
[9] S.G. Kandlikar (Ed.), Proceedings of the 2nd International Conference on Microchannels and MinASME, ASME, Rochester, NY, 2004.
[10] J. Pettersen, Flow vaporization of CO_2 in microchannel tubes, Ph.D. thesis, NTNU Trondheim, Norway, February 2002.
[11] D. Gorenflo, Behältersieden (Sieden bei freier Konvektion), in: VDI Wärmeatlas, sixth ed., VDI Verlag, 1991 (Chapter Ha1–Ha26).
[12] X.F. Peng, H.Y. Hu, B.X. Wang, Boiling nucleation during liquid flow in microchannels, Int. J. Heat Mass Transfer 41 (1) (1998) 101–106.
[13] L. Zhang et al., Enhanced nucleate boiling in microchannels, in: Proceedings of the IEEE Conference on Micro Electro Mechanical Systems (MEMS), 2002, pp. 89–92.
[14] Y. Zhao et al., Flow boiling of CO_2 in microchannels, ASHRAE Trans. 106 (2000) 437–445.
[15] Y.P. Peles, L.P. Yarin, G. Hetsroni, Evaporating two-phase flow mechanism in micro-channelsSymposium on Design, Test and Microfabrication of MEMS and MOEMS, 3680, SPIE, Paris, France, 1999, pp. 226–236.
[16] L. Jiang, M. Wong, Y. Zohar, A micro-channel heat sink with integrated temperature sensors for phase transition study, in: Proceedings of the IEEE Conference on Micro Electro Mechanical Systems (MEMS), 1999, pp. 159–164.
[17] L. Jiang, M. Wong, Y. Zohar, Phase change in microchannel heat sink under forced convection boiling, in: Proceedings of the IEEE Conference on Micro Electro Mechanical Systems (MEMS), 2000, pp. 397–402.
[18] T.S. Ravigururajan, Two-phase flow characteristics of refrigerant flows in a microchannel heat exchanger, Enhanced Heat Transfer 6 (1999) 419–427.
[19] S. Grohmann, Distributed cooling in cryogenics with miniaturized fluid circuits, Ph.D. thesis, Fortschritt-Berichte VDI, No. 148 in series 19, VDI Verlag, 2004.
[20] K. Borer et al., RD39, Status Report CERN/LHCC 2002-004, CERN (2002).
[21] K. Borer et al., RD39, Status Report CERN/LHCC 2003-060, LHCC-RD-003, CERN (2003).
[22] K. Borer et al., RD39, Status Report CERN/LHCC 2004-034, LHCC-RD-006, CERN (2004).
[23] S.G. Kandlikar, J. Shailesh, T. Shurong, Effect of surface roughness on heat transfer and fluid flow characteristics at low Reynolds numbers in small diameter tubes, Heat Transfer Eng. 24 (3) (2003) 4–16.
[24] D. Steiner, Wärmeübergang beim Sieden gesättigter Flüssigkeiten, in: VDI Wärmeatlas, 6th ed., VDI Verlag, 1991 (Chapter Hbb1–Hbb35).
[25] B. Perea Solano, Cryogenic silicon microstrip detector modules for the LHC, Ph.D. thesis, Universitat Politècnica de Catalunya, Escola Tècnica Superior d'Enginyeria Industrial de Barcelona ETSEIB, 2004.